Surface & Coatings Technology 454 (2023) 129195

Contents lists available at ScienceDirect

Surface & Coatings Technology

journal homepage: www.elsevier.com/locate/surfcoat

Significant improvement in surface hardness of Zr-based metallic glass by nanosecond pulsed laser irradiation in graphite powder water suspension

Hongyang Zhang [a], Yongfeng Qian [a], Lin Zhang [b], Minqiang Jiang [c,d], Hu Huang [a,*], Jiwang Yan [b]

[a] Key Laboratory of CNC Equipment Reliability, Ministry of Education, School of Mechanical and Aerospace Engineering, Jilin University, Changchun, Jilin 130022, China
[b] Department of Mechanical Engineering, Faculty of Science and Technology, Keio University, Yokohama 223-8522, Japan
[c] State Key Laboratory of Nonlinear Mechanics, Institute of Mechanics, Chinese Academy of Sciences, Beijing 100190, China
[d] School of Engineering Science, University of Chinese Academy of Sciences, Beijing 100049, China

ARTICLE INFO

Keywords:
Metallic glasses
Laser processing
Nanoindentation
Hardness
Serrated flow
Shear band

ABSTRACT

Metallic glasses (MGs) have shown promising application prospects as structural materials due to their unique mechanical properties. While, for broadening their application as functional materials, significant improvement in surface hardness of MGs is required. Accordingly, in this study, laser carbonization of MGs was attempted by irradiating the Zr-based MG surface immersed in graphite powder water suspension using a nanosecond pulsed laser. Nanoindentation response and surface morphologies of the initial and irradiated surfaces were characterized in detail. The results indicated that the hardness of the laser-irradiated surfaces was increased by 130 %–200 % (from 6.407 GPa to 19.193 GPa), and as well, the serrated flows in load-depth curves and the surface shear bands around the residual indent disappeared, suggesting the change in micro-scale plastic deformation behaviors of the laser-irradiated surfaces. Furthermore, the chemical composition of the initial and irradiated surfaces was analyzed by X-ray diffraction (XRD) and energy dispersive spectrometer (EDS), which showed that the irradiated surfaces were carbonized in the graphite powder water suspension. Accordingly, the increase in surface hardness was due to the formation of the hard crystalline phases.

1. Introduction

Metallic glasses (MGs) have long-range disordered and short-range ordered atomic arrangement structures, which allows them to avoid inherent defects of crystalline metals such as dislocation and grain boundary [1], and endues them with high hardness, excellent wear resistance, and so on [2–4]. However, MGs show typical brittle fracture characteristics under extreme load-bearing conditions due to the rapid propagation of single or several shear bands [5]. The limited plastic deformation ability restricts the application of MGs as structural materials. However, from the perspective of broadening the functional applications of MGs, it is still required to significantly improve their surface hardness.

Traditional quenching is not suitable for hardening the MGs due to the high temperature and long hours of heating. For most MGs, the glass forming ability is limited [6] and the supercooled liquid region is quite narrow [7], so innovative surface hardening methods need to be explored urgently for MGs. Pulsed lasers with features of extremely fast heating and cooling have been widely used for processing MGs. For instance, laser-induced ripples [8] and Saffman-Taylor fingering [9] are meaningful for the fundamental understanding of laser-material interaction. Furthermore, functional surfaces with hydrophobicity, structural color, and hierarchical micro/nanostructures have been fabricated on MGs by pulsed laser irradiation [10–12]. Moreover, pulsed laser surface processing including laser polishing [13,14], laser shock peening [15,16] and laser-induced secondary phase [17] could tune the mechanical properties of materials. For example, in one previous study [18], by nanosecond pulsed laser irradiation of Zr-based MG surface in flowing nitrogen, ZrN phase was introduced into the amorphous matrix and the surface was hardened. However, the increase in surface hardness was still limited. Therefore, it is necessary to develop more effective methods to significantly improve the hardness of Zr-based MG.

Zr-based MG is a typical and prominent MG, which can be cast in fully amorphous rods up to 14 mm in diameter at a cooling rate of approximately 1 K/s [19,20]. Due to their superior mechanical properties and high forming ability, Zr-based MGs become candidate

* Corresponding author.
E-mail address: huanghu@jlu.edu.cn (H. Huang).

https://doi.org/10.1016/j.surfcoat.2022.129195
Received 21 October 2022; Received in revised form 3 December 2022; Accepted 21 December 2022
Available online 30 December 2022

materials for mechanical and aerospace applications such as high-strength gears, micro-engine components, turbocharger wheels, turbine blades, as well as fishing rods, golf club shafts and club heads in sporting products [21]. Laser carbonization will be a possible approach to further expand the application of Zr-based MG as functional materials. Laser carbonization has proven to be an ideal hardening method for diverse metal materials such as titanium, aluminum, and steel via pre-coating carbon layers or controlling gas atmospheres [22–24]. However, the pre-coated layer was easily blown away from the substrate during the laser processing, failing large-area carbonization. When laser carbonization was achieved by controlled gas atmospheres, flammable, explosive, or toxic gases, such as propylene (C3H6) and propane (CH3CH2CH3), were usually used. This required not only a high-vacuum chamber but also post-treatment of the waste gas, which undoubtedly increased the experimental difficulty. In one previous study on the microelectrical discharge machining (micro-EDM) of Zr-based MG [25], the machined surface had been carbonized when the dielectric was EDM oil. Both the EDM process and laser process would generate high temperature, and the materials were molted and vaporized, which provides the possibility for laser carbonization of Zr-based MG. Nevertheless, the hardening effect of laser carbonization of Zr-based MG still requires experimental studies, and whether the quality of the carbonized surface will meet the demands of practical applications is not yet known.

In this paper, to explore the feasibility of laser carbonization of Zr-based MG as well as its effects on surface properties, the nanosecond pulsed laser was employed to irradiate the Zr-based MG which was immersed in graphite powder water suspension. The flowing suspension carrying graphite was readily supplemented to the position in which the laser spot moved, providing sufficient carbon element for the carbonization reaction, and also the experimental setup was simple and easy to perform. The resultant surface characteristics were investigated in detail, and the results indicated that laser carbonization had been successfully implemented for the Zr-based MG, which significantly improved its surface hardness from 6.407 GPa to 19.193 GPa.

2. Materials and methods

2.1. Material preparation

The commercial MG Vitreloy 1 ($Zr_{41.2}Ti_{13.8}Cu_{12.5}Ni_{10}Be_{22.5}$, in at.%) with cross section of 20 mm × 20 mm and thickness of 2 mm was purchased from PESHING NEW METAL, China. It was produced by arc melting of Zr, Ti, Cu, Ni, and Be raw materials (>99.9 wt% purity), followed by copper die casting in an argon atmosphere. The ingots were remelted five times to obtain MG samples with homogeneous composition. Prior to laser irradiation, the sample was ground by using 400, 1200, and 2000 grit SiC sandpapers to remove the surface oxide layer. Then, the sample was polished to a mirror face with diamond paste and cleaned with ethanol. The raw graphite powder was manually milled for an hour, and the morphology is shown in Fig. 1. The milled graphite powder and deionized water were mixed in a beaker with the weight ratio of 1:7 and stirred thoroughly. The beaker was further ultrasonically vibrated to make the graphite powder uniformly disperse in the water suspension. The graphite powder and deionized water would provide enough carbon element and restrict the expansion of laser-induced plasma [26], respectively.

2.2. Experimental device and processing parameters

Fig. 2 presents the schematic diagram of the nanosecond pulsed fiber laser system and the scanning strategy. Firstly, the Zr-based MG sample was fixed in a circular transparent container, and the sample surface was adjusted to be nearly on the focal plane of the laser beam. Then, the pre-configured graphite powder water suspension was dropped into the container, and the liquid level was controlled to be 1 mm higher than the sample surface. After that, the nanosecond pulsed laser (SP-050P-A-EP-Z-F-Y, SPI, UK) with a wavelength of 1064 nm was employed for subsequent laser irradiation. The spot diameter, repetition frequency, and pulse width of the laser beam are 43 μm, 600 kHz, and 7 ns, respectively. As shown in Fig. 2, each scanning region is square with a size of 2 mm × 2 mm. The first line scans from left to right, and the next line moves along the feed direction by an adjustable interval (namely, Δy). The variation in overlap ratio was realized by adjusting the interval between adjacent lines. Through preliminary experiments, the following laser irradiation parameters were selected: laser power of 3.24 W, scanning speed of 5 mm/s and number of irradiation cycle of 1. Four experimental cases were designed with overlap ratios of 30 % (case 1), 50 % (case 2), 70 % (case 3), and 90 % (case 4), respectively. In order to ensure comparability of the entire study, all experiments were conducted on the same sample.

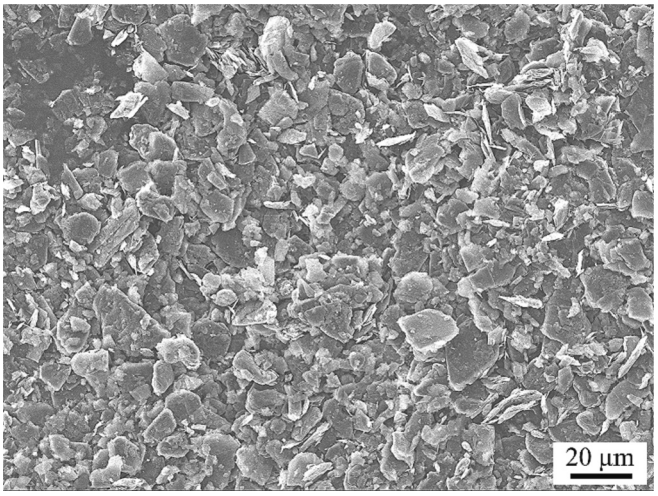

Fig. 1. Morphology of the milled graphite powder.

2.3. Surface characterization

After laser irradiation, the irradiated surfaces were polished again to obtain smooth surfaces for subsequent characterization. A tungsten filament scanning electron microscope (SEM, JSM-IT500A, JEOL, Japan) equipped with an energy dispersive spectrometer (EDS, EX-74600U4L2Q, JEOL, Japan) was employed to obtain the morphologies of the irradiated surfaces. The acceleration voltage, working distance, and photo time in SEM were 10 kV, 9.8 mm, and 40 s, respectively. The phase components of initial and irradiated surfaces were analyzed via X-ray diffraction (XRD, D8 Discover, Bruker, Germany) with a Cu Kα (λ = 1.54 Å) radiation. The voltage and current of the X-ray generator were 40 kV and 40 mA, respectively, and the rotation angle (2θ) was in the range of 20° to 80° with a scanning speed of 4°/min. The atomic percent was measured by EDS with an acceleration voltage of 15 kV. The nanoindentation response of the initial and irradiated surfaces was measured by a nanoindentation tester (DUH-211 s, Shimadzu, Japan), which was equipped with a triangular pyramid indenter with a face angle of 115°. The load-unload testing mode was selected. For comparison, the indentation loads of 150 mN and 200 mN were chosen respectively. The loading and unloading rates were 10 mN/s, and the holding time at the maximum load was 5 s. To ensure the accuracy of hardness measurement, 10 indentation tests were performed for each case. According to the load-depth curves, the nanoindentation hardness was calculated by means of the Oliver-Pharr's (OP's) method [27].

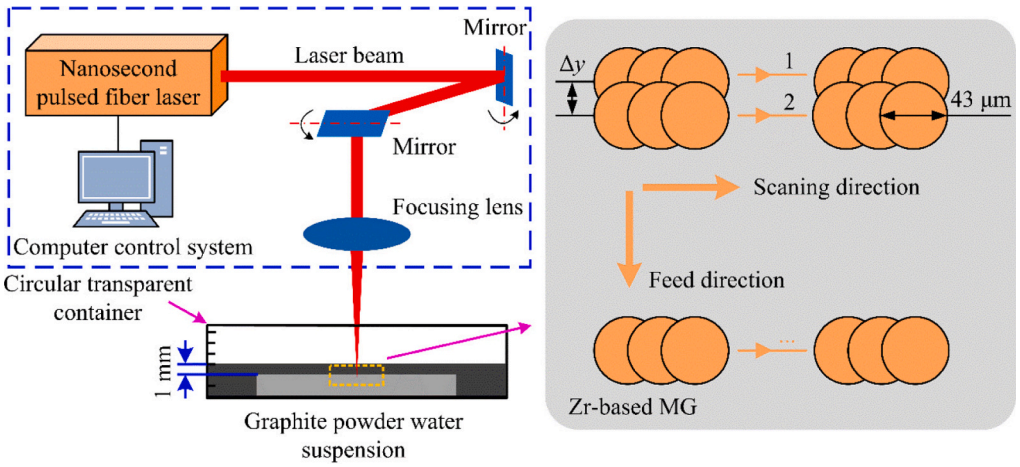

Fig. 2. Schematic diagram of the nanosecond pulsed laser irradiation system and the scanning strategy.

3. Results

3.1. Microstructure and chemical composition

Fig. 3(a)-(d) show the SEM morphologies of the polished surfaces after laser irradiation under the overlap ratios of 30 %, 50 %, 70 %, and 90 %, which correspond to cases 1, 2, 3, and 4, respectively. Regular scanning tracks and local pores can be observed in case 1 with the overlap ratio of 30 %. As the overlap ratio increases from 50 % to 70 % and then to 90 % (cases 2, 3 and 4), the scanning tracks become increasingly irregular or even indistinguishable, and the irradiated surfaces gradually become unsmooth with more pores and visible cracks

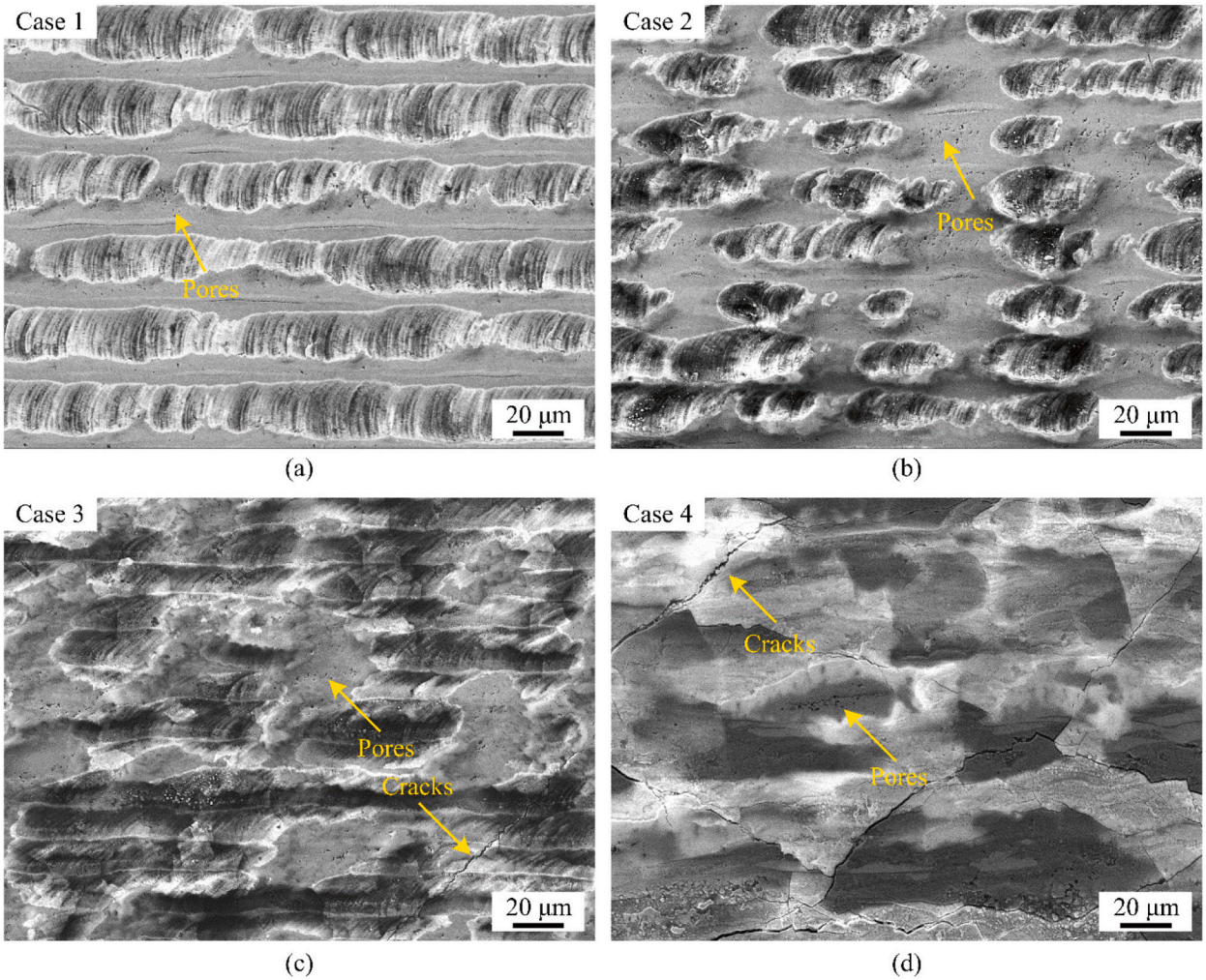

Fig. 3. SEM morphologies of the irradiated surfaces (after polishing) obtained under different overlap ratios: (a) 30 %, (b) 50 %, (c) 70 %, and (d) 90 %. The other parameters (laser power of 3.24 W, scanning speed of 5 mm/s and number of irradiation cycle of 1) were the same.

appearing.

Fig. 4 shows the XRD patterns of the sample before and after laser irradiation. Broad humps are observed on the XRD patterns of all detected cases, indicating that the amorphous phase is still maintained for all the irradiated surfaces. However, several sharp peaks corresponding to ZrC, TiC and ZrO_2 phases [28–30] appear on the XRD patterns of the irradiated surfaces, which demonstrates that the irradiated surfaces have been carbonized but accompanied by oxidation. With laser irradiation, C and O atoms can be decomposed in the graphite powder water suspension [25]. Due to the high chemical affinity of C and O with Zr and Ti [31,32], the MG matrix element would react with C and O atoms under high temperature condition, forming ZrC, TiC, and ZrO_2 phases. Additionally, for all XRD patterns, there is only a slight difference in intensity but no difference in peak position.

3.2. Nanoindentation hardness

Fig. 5(a) presents the SEM morphology of case 1 and the positions for nanoindentation testing. These tests were performed on the smooth area with a width of approximately 10 μm between adjacent tracks. In order to study the effect of laser irradiation, the hardness of initial and irradiated surfaces was tested, and the results are displayed in Fig. 5(b). Among cases 1 to 4, the maximum average hardness is obtained with case 1 (19.193 GPa), and the minimum average hardness is obtained with case 4 (15.091 GPa). Compared with the initial surface hardness of 6.407 GPa, the hardness is significantly increased by 130 %–200 %. Meanwhile, nanoindentation tests with a higher load of 200 mN were also performed to verify the hardening role. As shown in Fig. 5(c), the obtained hardness is lower than that obtained under 150 mN, which could be due to (1) the indentation size effect (ISE) [33] and (2) the weakened hardening role along the depth direction. However, the hardness of all the irradiated surfaces obtained under 200 mN is still beyond 10 GPa and the variation tendency in hardness is consistent with that measured under 150 mN. The above results indicate that nanosecond pulsed laser irradiation in graphite powder water suspension can significantly improve the surface hardness of Zr-based MG.

In order to verify the effect of surface hardening, representative cases 1 and 4 with the highest and lowest average hardness are selected for comparative analysis. From the load-depth curves of the as-cast MG, case 1 and case 4 shown in Fig. 6(a), it can be observed that the residual indent depth of as-cast MG is 786 nm, while the residual indent depths of case 1 and case 4 are 467.6 nm and 481.4 nm, respectively. The residual indent depth of the initial surface is obviously larger than that of the irradiated surfaces, further confirming the hardening effect of the laser irradiated surfaces. Additionally, as the hardness calculated by the OP's method could be affected by the pile-ups around the indent [34], Meyer's hardness law was also employed to calculate the surface hardness according to the following formula [35]

$$H_M = \frac{P_{max}}{A} \quad (1)$$

where H_M represents the Meyer's hardness (GPa), P_{max} is the maximum load (mN), and A is the projected area (mm^2) calculated by the residual indent morphology. According to formula (1), the hardness of 10 tests is obtained for the as-cast MG, case 1 and case 4. Fig. 6(b) displays the statistical results of the Meyer's and OP's hardness, and their average values are listed in Table 1. Although the OP's hardness is slightly larger than the Meyer's hardness due to the effect of pile-ups, their variation tendency is consistent. Nevertheless, the comparison in Meyer's hardness further directly verifies the hardening effect for Zr-based MG by nanosecond pulsed laser irradiation in graphite powder water suspension.

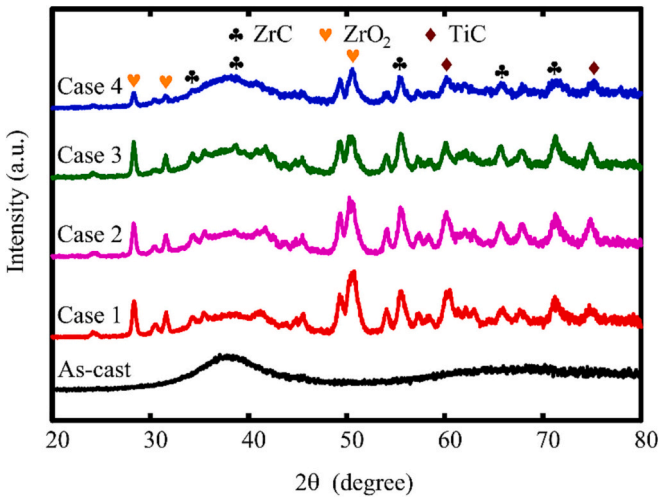

Fig. 4. XRD patterns of the as-cast MG as well as the laser irradiated surfaces.

3.3. Serrated flow and shear bands

The improvement in surface hardness will inevitably affect the micro-scale plastic deformation behaviors of MGs, which can be directly reflected by the serrated flows in load-depth curves [36]. It is well known that for nanoindentation of MGs, a relatively high loading rate would suppress the serrated flow and a relatively low loading rate would promote the serrated flow [37–39]. Therefore, the loading rate of 1 mN/s was selected for easily characterizing the serrated flow of the irradiated surfaces, and the results are presented in Fig. 7. The locally enlarged view in the range of 90 to 150 mN in the load-depth curve of as-cast MG is inserted into Fig. 7(a). Obvious depth displacement bursts can be observed in the local enlarged load-depth curve, which is the so-called serrated flow behavior during nanoindentation testing of MGs [40]. However, for the irradiated surfaces, the load-depth curves shown in Fig. 7(c) and (e) are quite smooth without conspicuous serrated flow. In order to further characterize the serrated flow, the depth difference-load curves are given in Fig. 7(b), (d) and (f) according to the depth-difference method [41], and each sharp peak represents a serrated flow in the load-depth curve. In the load range of 10–150 mN, the depth difference-load curve of the as-cast MG surface has 29 peaks with the depth difference being >2 nm; while the depth difference-load curves of the irradiated surfaces are quite smooth, and there are almost no peaks over 2 nm. The disappearance of serrated flow suggests that nanosecond pulsed laser irradiation of Zr-based MG in graphite powder water suspension also changes the micro-scale plastic deformation behaviors of Zr-based MG.

According to some previous studies [42,43], the variation of the serrated flow is related to the shear banding events. As shown in Fig. 8, prominent shear bands appear around the residual indent of the as-cast MG surface. On the contrary, neither case 1 nor case 4 has visible surface shear bands. Additionally, the size of the residual indent is greatly different. The average length of three sides of the residual indent for as-cast MG is 7.68 μm; while the average lengths of three sides for case 1 and case 4 are 5.65 μm and 5.75 μm, respectively. With consideration of the change in serrated flow in Fig. 7, it is concluded that nanosecond pulsed laser irradiation of Zr-based MG in graphite powder water suspension prevents the generation of surface shear bands and changes the micro-scale plastic deformation behavior of Zr-based MG during nanoindentation.

4. Discussion

4.1. Hardening mechanism

From the above experimental results, it is noted that under the employed experimental conditions, the maximum average hardness of

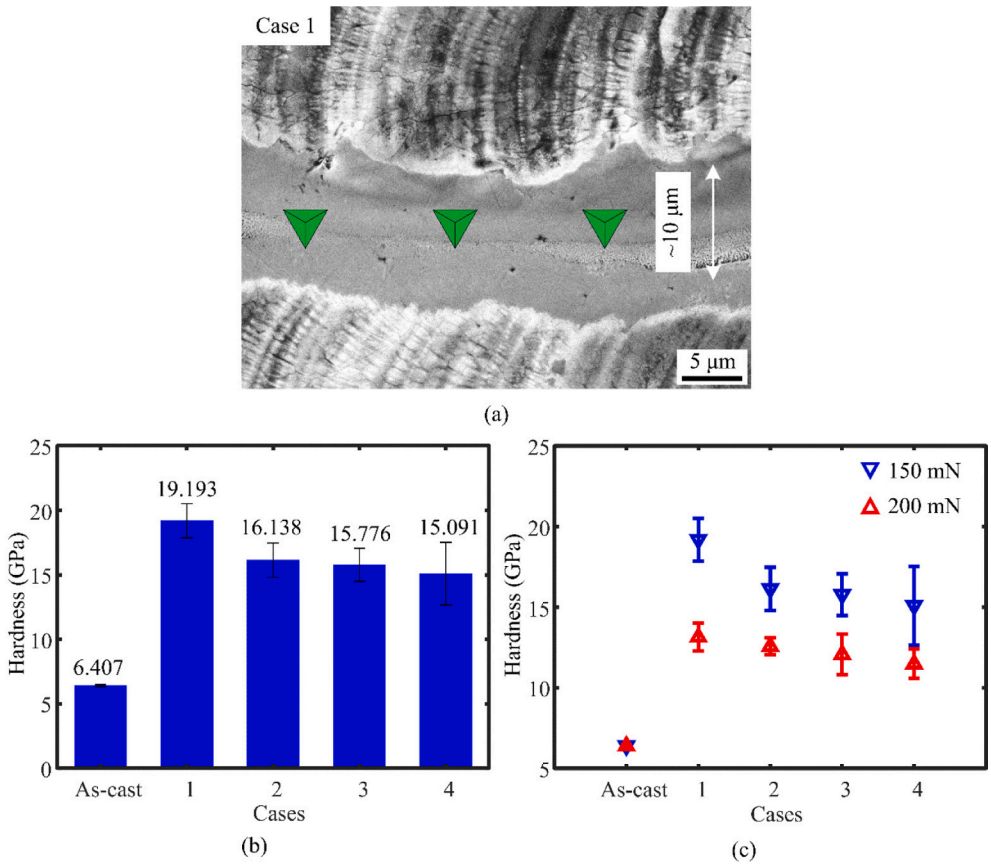

Fig. 5. (a) SEM morphology of case 1 and the positions for nanoindentation testing; (b) hardness results of as-cast MG and cases 1 to 4 obtained under 150 mN; (c) comparison in hardness obtained under 150 mN and 200 mN.

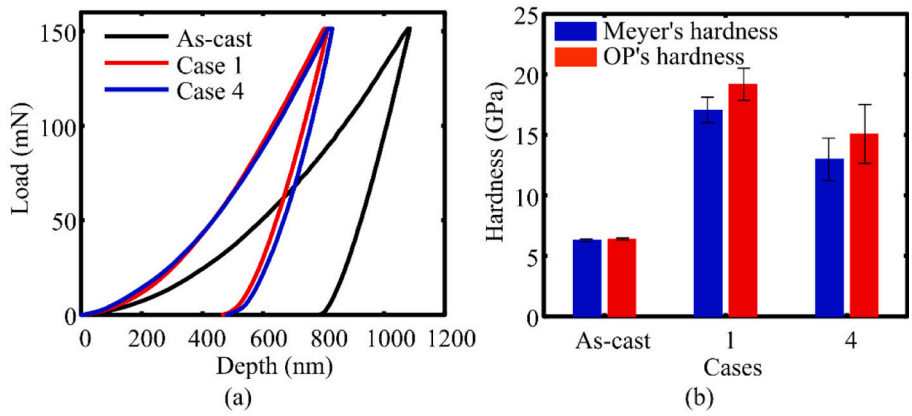

Fig. 6. (a) Load-depth curves of the as-cast MG, case 1 and case 4; (b) statistical results of the Meyer's and OP's hardness for as-cast MG, case 1 and case 4.

Table 1
The average values of Meyer's and OP's hardness obtained by 10 tests.

	Meyer's hardness (GPa)	OP's hardness (GPa)
As-cast	6.297	6.407
Case 1	17.074	19.193
Case 4	12.995	15.091

the irradiated surfaces is 19.193 GPa and the minimum average hardness is 15.091 GPa, which is increased by 130 %–200 % than the initial surface hardness of 6.407 GPa. By changing the laser irradiation parameters, different degrees of hardened surfaces can be achieved. The XRD patterns shown in Fig. 4 indicate similar crystalline phases of the irradiated surfaces. In order to quantitatively analyze the chemical composition, the atomic percent of each element was characterized by EDS point analysis with per point analysis time of 150 s. The position for point analysis and the variation tendency in each element are presented in Fig. 9(a) and (b), respectively. The average value of three EDS testing points is regarded as the atomic percent of each case. As listed in Table 2, for all irradiated surfaces, the carbon atomic percent is over 50 %. When the content of carbon element exceeds a critical value, the increase of carbon element will not participate in laser carbonization but it will remain on the irradiated surfaces in the form of elemental carbon [25]. Therefore, the increase in surface hardness after laser irradiation is

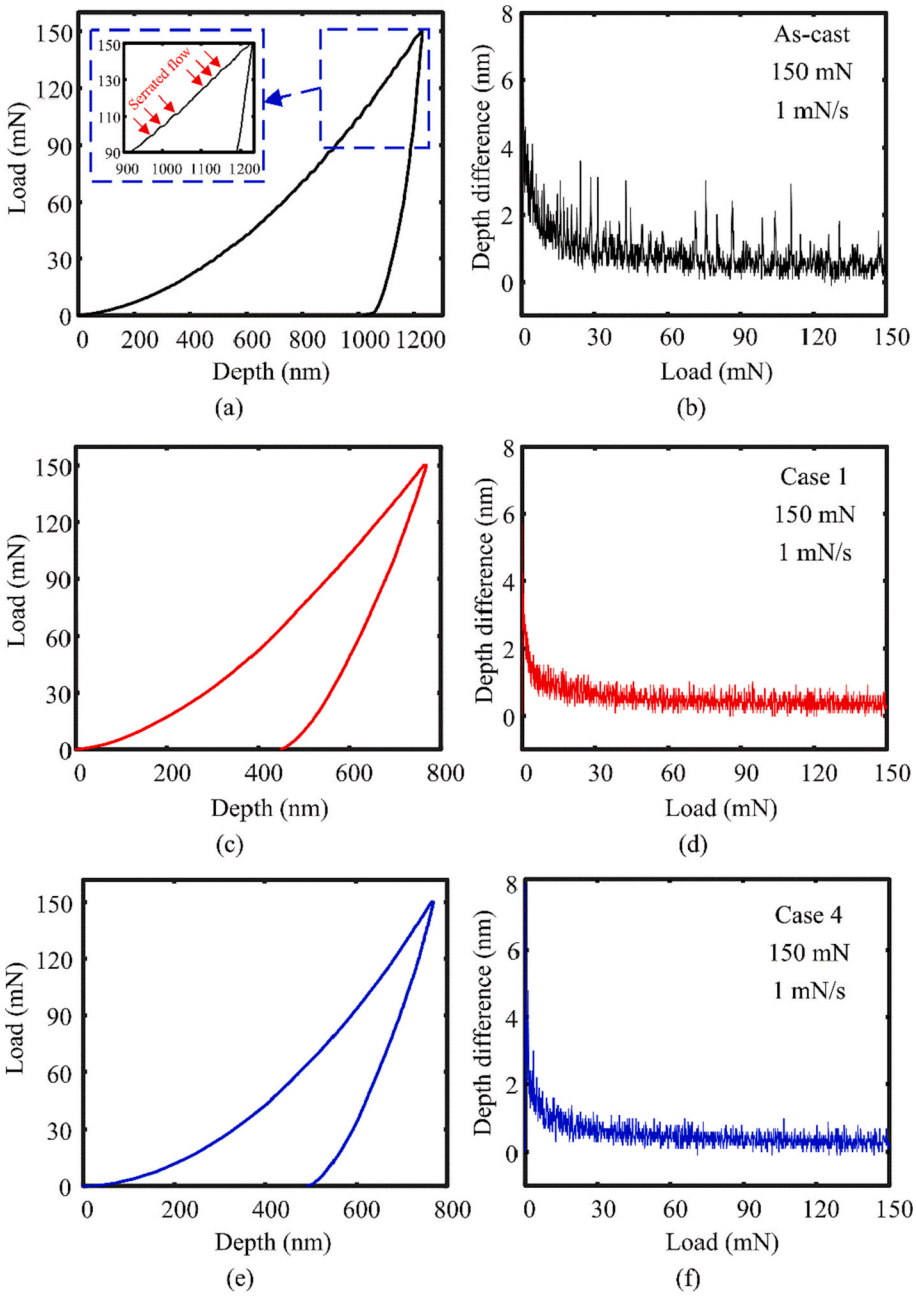

Fig. 7. Load-depth curves and depth difference-load curves: (a-b) as-cast MG, (c-d) case 1, and (e-f) case 4.

mainly due to the introduction of the crystalline phases of ZrC, TiC and ZrO_2 [18,44]. These crystalline phases formed in the MG matrix impede the initiation and propagation of shear bands, thus increasing the resistance to plastic deformation and hardening the MG surface. Moreover, the hardness of ZrC, TiC, and ZrO_2 phases is much higher than MG, further contributing to the increase in surface hardness. The above phenomena indicate that laser carbonization has been successfully achieved on Zr-based MG surface and significantly improved its surface hardness. Generally, by increasing the overlap ratio, the surface hardness would be improved, but this tendency does not appear in the current work. In Fig. 3, it is noted that the irradiated surface (after polishing) of case 1 is relatively smooth and flat; on the contrary, the surfaces of cases 2–4 are very rough with pores and cracks. The rough surface caused by laser ablation will increase the absorption of subsequent laser energy, further resulting in more pores and visible cracks [45]. By analyzing the SEM morphologies in Fig. 3, it is suggested that these increasing pores and cracks caused by the increase of overlap ratio would reduce the densification of the irradiated surfaces, thereby weakening the effect of surface hardening. The relatively poor surface quality should be the main reason leading to the surface hardness of cases 2–4 being less than that of case 1.

4.2. *Tuning of the micro-scale plastic deformation behaviors*

Nanosecond pulsed laser irradiation in graphite powder water suspension not only improves the surface hardness of Zr-based MG, but also changes the micro-scale plastic deformation behaviors. It is well-known that shear bands are the main carrier for the micro-scale plastic deformation of MGs [46,47]. For the as-cast MG surface, there are fluctuations in the load-depth curve in Fig. 7(a) and sharp peaks in the depth difference-load curve in Fig. 7(b). Prominent shear bands can be observed around the residual indent of the as-cast MG surface in Fig. 8

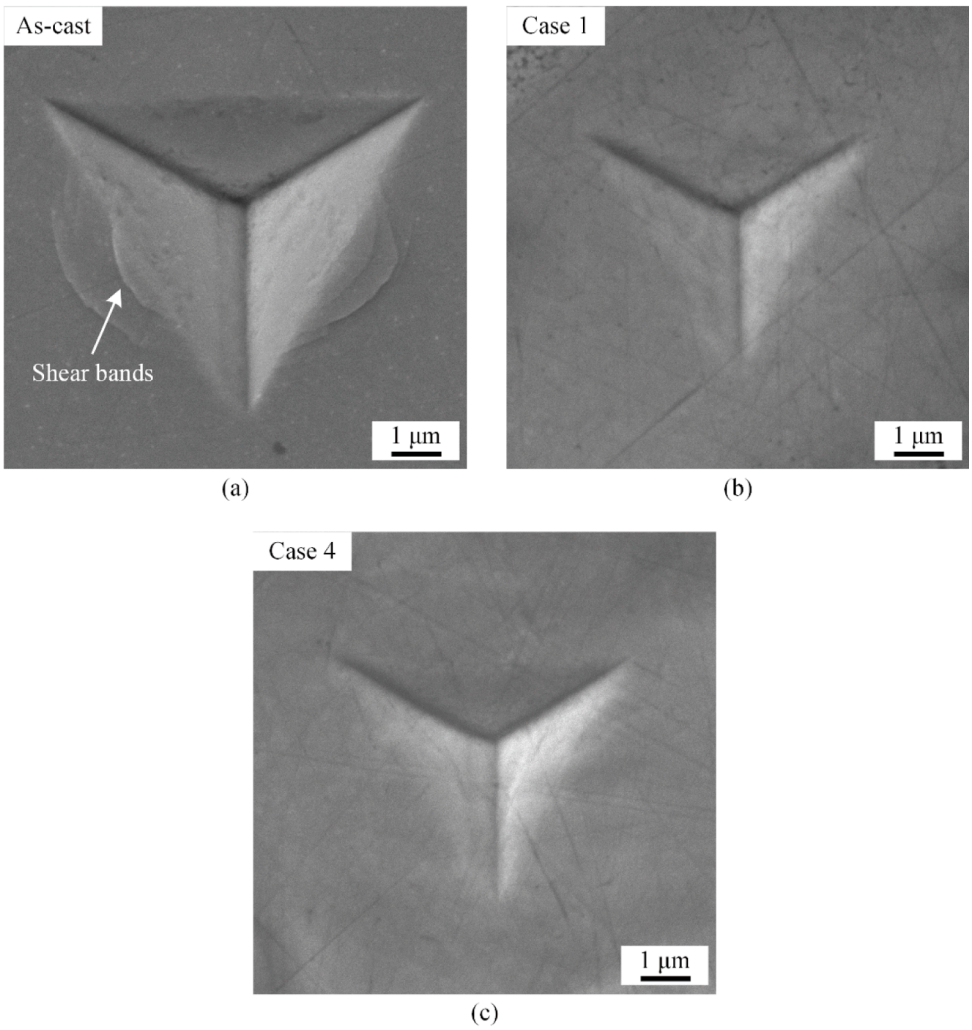

Fig. 8. SEM morphologies of the residual indents: (a) as-cast MG, (b) case 1, and (c) case 4.

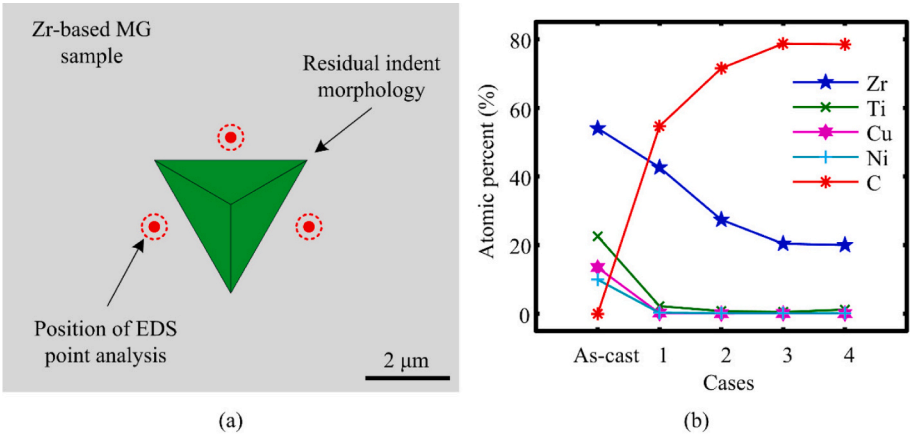

Fig. 9. (a) Position schematic diagram of the EDS point analysis; (b) variation tendency of each element of the as-cast MG as well as the laser irradiated surfaces.

(a). However, there are no fluctuations in the load-depth curves of Fig. 7 (c) and (e) and no sharp peaks in the depth difference-load curves of Fig. 7(d) and (f). No surface shear bands can be observed around the residual indents of the carbonized surfaces in Fig. 8(b) and (c). The nanoindentation response indicates that the introduction of crystalline phases impedes the initiation and propagation of surface shear bands and plays an important role in tuning the micro-scale plastic deformation behaviors of Zr-based MG.

5. Conclusions

In summary, by nanosecond pulsed laser irradiation in graphite

Table 2
Atomic percent of each element of the as-cast MG and laser irradiated surfaces obtained from three EDS testing points for each case (analysis time of 150 s per point).

	Zr	Cu	Ni	Ti	C
As-cast	54.03	13.45	9.95	22.57	0
Case 1	42.66	0.16	0.29	2.23	54.67
Case 2	27.4	0.05	0.2	0.81	71.54
Case 3	20.42	0.11	0.21	0.54	78.72
Case 4	20.03	0.09	0.19	1.2	78.5

powder water suspension, laser carbonization was attempted on the Zr-based MG to improve its surface hardness. Through experiments and analysis, the following conclusions could be obtained.

(1) Laser carbonization of Zr-baed MG was achieved by laser irradiation in graphite powder water suspension. Compared to the as-cast surface, the hardness of the carbonized MG surface was increased by 130 %–200 %.
(2) By changing the overlap ratio, the hardening degree could be adjusted. With a 30 % overlap ratio, the hardness of the carbonized surface was 19.193 GPa. When increasing the overlap ratio to 90 %, the hardness was decreased to 15.091 GPa.
(3) ZrC, TiC, and ZrO_2 crystalline phases were generated on the laser irradiated surfaces. These crystalline phases not only increased the surface hardness but also tuned the micro-scale plastic deformation behaviors of Zr-based MG surface.

This study demonstrates that laser carbonization can significantly increase the surface hardness of Zr-based MG, which will greatly expand its application as surface functional materials. Nevertheless, pores and cracks are observed in the surface morphologies, decreasing the densification of the carbonized surface. In future study, the surface quality of laser carbonized MG will be further improved to meet the demands of practical applications.

CRediT authorship contribution statement

Hongyang Zhang: Investigation, Formal analysis, Data curation, Writing – original draft. **Yongfeng Qian:** Investigation, Data curation. **Lin Zhang:** Investigation, Data curation. **Minqiang Jiang:** Methodology. **Hu Huang:** Conceptualization, Data curation, Funding acquisition, Methodology, Resources, Supervision, Writing – review & editing. **Jiwang Yan:** Methodology, Supervision.

Declaration of competing interest

The authors declare that they have no known competing financial interests or personal relationships that could have appeared to influence the work reported in this paper.

Data availability

Data will be made available on request.

Acknowledgement

This work was supported by the Natural Science Foundation of Jilin Province (20220101198JC), the National Natural Science Foundation of China (Grant No. 51705197), National Outstanding Youth Science Fund Project (No. 12125206) of NSFC, the Opening Project of the Key Laboratory of CNC Equipment Reliability, Ministry of Education, Jilin University (JLU-cncr-202208), and the Fundamental Research Funds for the Central Universities (2020-2022).

References

[1] M.M. Khan, A. Nemati, Z.U. Rahman, U.H. Shah, H. Asgar, W. Haider, Recent advancements in bulk metallic glasses and their applications: a review, Crit. Rev. Solid State Mater. Sci. 43 (2018) 233–268.
[2] J. Lindwall, V. Pacheco, M. Sahlberg, A. Lundback, L.E. Lindgren, Thermal simulation and phase modeling of bulk metallic glass in the powder bed fusion process, Addit. Manuf. 27 (2019) 345–352.
[3] Y.Y. Shen, Y.Q. Li, H.L. Tsai, Effect of pre-existing nuclei on crystallization during laser welding of Zr-based metallic glass, J. Non-Cryst. Solids 513 (2019) 55–63.
[4] L.W. Hu, X. Liu, C. Liang, S. Zhao, T. Chen, J. Li, G. Le, F. Qu, Y. Zhou, L. Qi, D. Wang, Microstructure evolution and corrosion mechanism of laser cladded Zr-Cu-Ni-Al in-situ metallic glass matrix composite coatings, Surf. Coat. Technol. 409 (2021), 126908.
[5] Y.H. Liu, G. Wang, R.J. Wang, D.Q. Zhao, M.X. Pan, W.H. Wang, Super plastic bulk metallic glasses at room temperature, Science 315 (2007) 1385–1388.
[6] Z. Li, Z. Huang, F. Sun, X. Li, J. Ma, Forming of metallic glasses: mechanisms and processes, Mater. Today Adv. 7 (2020), 100077.
[7] G. Kaltenboeck, T. Harris, K. Sun, T. Tran, G. Chang, J.P. Schramm, M. D. Demetriou, W.L. Johnson, Accessing thermoplastic processing windows in metallic glasses using rapid capacitive discharge, Sci. Rep. 4 (2014) 6441.
[8] Y. Liu, M.Q. Jiang, G.W. Yang, Y.J. Guan, L.H. Dai, Surface rippling on bulk metallic glass under nanosecond pulse laser ablation, Appl. Phys. Lett. 99 (2011), 191902.
[9] Y. Liu, M.Q. Jiang, G.W. Yang, J.H. Chen, Y.J. Guan, L.H. Dai, Saffman-Taylor fingering in nanosecond pulse laser ablating bulk metallic glass in water, Intermetallics 31 (2012) 325–329.
[10] H. Huang, J.W. Yan, Surface patterning of zr-based metallic glass by laser irradiation induced selective thermoplastic extrusion in nitrogen gas, J. Micromech. Microeng. 27 (2017), 075007.
[11] Q. Gao, D. Ouyang, X.T. Liu, S.X. Wu, X. Huang, N. Li, Fabricating colorful bulk metallic glass surfaces by femtosecond laser processing, Mater. Chem. Phys. 266 (2021), 124561.
[12] H. Huang, N. Jun, M.Q. Jiang, M. Ryoko, J.W. Yan, Nanosecond pulsed laser irradiation induced hierarchical micro/nanostructures on zr-based metallic glass substrate, Mater. Des. 109 (2016) 153–161.
[13] C.P. Ma, Y.C. Guan, W. Zhou, Laser polishing of additive manufactured Ti alloys, Opt. Lasers Eng. 93 (2017) 171–177.
[14] D. Kang, P. Zou, H. Wu, W.J. Wang, J.L. Xu, Research on ultrasonic vibration-assisted laser polishing of the 304 stainless steel, J. Manuf. Process. 62 (2021) 403–417.
[15] F.W. Wang, X.L. Yan, L. Liu, M. Nastasi, Y.F. Lu, B. Cui, Surface strengthening of single-crystal alumina by high-temperature laser shock peening, Mater. Res. Lett. 9 (2020) 155–161.
[16] Y.S. Li, K. Zhang, Y. Wang, W.Q. Tang, Y.T. Zhang, B.C. Wei, Z. Hu, Abnormal softening of Ti-metallic glasses during nanosecond laser shock peening, Mater. Sci. Eng. A 773 (2020), 138844.
[17] Y. Chen, C.G. Tang, J.Z. Jiang, Bulk metallic glass composites containing B2 phase, Prog. Mater. Sci. 121 (2021), 100799.
[18] H. Huang, M.Q. Jiang, J.W. Yan, The coupling effects of laser thermal shock and surface nitridation on mechanical properties of Zr-based metallic glass, J. Alloy. Compd. 770 (2019) 864–874.
[19] S.F. Hsieh, S.L. Chen, M.H. Lin, S.F. Ou, W.T. Lin, M.S. Huang, Crystallization and carbonization of an electrical discharge machined Zr-based bulk metallic glass alloy, J. Mater. Res. 28 (2013) 3177–3184.
[20] H.D. Yang, L.B. Zhang, J.S. Zhang, H.H. Tang, S.H. Chen, Effect of sample size and cooling rate on the plastic deformation behavior of bulk metallic glasses: a comparative study, J. Non-Cryst. Solids 589 (2022), 121643.
[21] W.Z. Wu, X.C. Li, Q.P. Liu, J.Y. Hsi Fuh, A.D. Zheng, Y.M. Zhou, L.Q. Ren, G.W. Li, Additive manufacturing of bulk metallic glass: principles, materials and prospects, Mater. Today Adv. 16 (2022), 100319.
[22] M. Bahiraei, Y. Mazaheri, M. Sheikhi, A. Heidarpour, Mechanism of TiC formation in laser surface treatment of the commercial pure titanium pre-coated by carbon using PVD process, J. Alloy. Compd. 834 (2020), 155080.
[23] F. Fariaut, C. Boulmer-Leborgne, E. Le Menn, T. Sauvage, C. Andreazza, P. Andreazza, C. Langlade, Surface carburization of aluminum alloys by excimer laser, Surf. Coat. Technol. 146 (2001) 324–330.
[24] N. Maharjan, W. Zhou, N.E. Wu, Direct laser hardening of AISI 1020 steel under controlled gas atmosphere, Surf. Coat. Technol. 385 (2020), 125399.
[25] H. Huang, J.W. Yan, On the surface characteristics of a Zr-based bulk metallic glass processed by microelectrical discharge machining, Appl. Surf. Sci. 355 (2015) 1306–1315.
[26] X. Song, X.Q. Wu, K.L. Xiao, C. Li, H.Y. Wang, M.Q. Jiang, Nanosecond laser ablation of a metallic glass in water: a high time-resolved imaging study, Philos. Mag. 100 (2020) 1–13.
[27] W.C. Oliver, G.M. Pharr, Measurement of hardness and elastic modulus by instrumented indentation: advances in understanding and refinements to methodology, J. Mater. Res. 19 (2011) 3–20.
[28] H.Q. Ding, S.Y. Jiang, J. Xu, Cavitation erosion resistance of ZrC nanoceramic coating, Proc. Inst. Mech. Eng. Part J. -J. Eng. Tribol. 234 (2020) 833–841.
[29] M.J. Hamedi, M.J. Torkamany, J. Sabbaghzadeh, Effect of pulsed laser parameters on in-situ TiC synthesis in laser surface treatment, Opt. Lasers Eng. 49 (2011) 557–563.
[30] Z. Hu, X.Q. Lei, Y. Wang, K. Zhang, Oxidation feature and diffusion mechanism of Zr-based metallic glasses near the glass transition point, Mater. Res. Express 5 (2018), 036511.

[31] J.K. Xu, Q.Q. Pei, Z.X. Lian, P. Yu, G.S. Ma, H.D. Yu, Experimental study on wire-electrical discharge machining of zirconium-based metallic glass, Mater. Res. Express 6 (2019), 115214.
[32] H. Kato, T. Hirano, A. Matsuo, Y. Kawamura, A. Inoue, High strength and good ductility of Zr55Al10Ni5Cu30 bulk glass containing ZRC particles, Scr. Mater. 43 (2000) 503–507.
[33] M.C. Li, M.Q. Jiang, F. Jiang, L. He, J. Sun, Testing effects on hardness of a Zr-based metallic glass under nanoindentation, Scr. Mater. 138 (2017) 120–123.
[34] A. Bolshakov, G.M. Pharr, Influences of pileup on the measurement of mechanical properties by load and depth sensing indentation techniques, J. Mater. Res. 13 (1998) 1049–1058.
[35] G. Berg, P. Grau, Meyer's hardness law and its relation to other measures of ball hardness tests, Cryst. Res. Technol. 32 (1997) 149–154.
[36] H. Huang, M.Q. Jiang, J.W. Yan, Softening of Zr-based metallic glass induced by nanosecond pulsed laser irradiation, J. Alloy. Compd. 754 (2018) 215–221.
[37] F. Li, M. Song, S. Ni, S.F. Guo, X.Z. Liao, Correlation between hardness and shear banding of metallic glasses under nanoindentation, Mater. Sci. Eng. A 657 (2016) 38–42.
[38] C.A. Schuh, T.G. Nieh, A nanoindentation study of serrated flow in bulk metallic glasses, Acta Mater. 51 (2003) 87–99.
[39] Y.I. Golovin, V.I. Ivolgin, V.A. Khonik, K. Kitagawa, A.I. Tyurin, Serrated plastic flow during nanoindentation of a bulk metallic glass, Scr. Mater. 45 (2001) 947–952.
[40] L. Cheng, Z.M. Jiao, S.G. Ma, J.W. Qiao, Z.H. Wang, Serrated flow behaviors of a Zr-based bulk metallic glass by nanoindentation, J. Appl. Phys. 115 (2014), 084907.
[41] H. Huang, H.W. Zhao, Z.Y. Zhang, Z.J. Yang, Z.C. Ma, Influences of sample preparation on nanoindentation behavior of a Zr-based bulk metallic glass, Materials 5 (2012) 1033–1039.
[42] A.L. Greer, Y.Q. Cheng, E. Ma, Shear bands in metallic glasses, Mater. Sci. Eng. R 74 (2013) 71–132.
[43] T.C. Hufnagel, C.A. Schuh, M.L. Falk, Deformation of metallic glasses: recent developments in theory, simulations, and experiments, Acta Mater. 109 (2016) 375–393.
[44] Y. Jiao, E. Brousseau, K. Kosai, A.J.G. Lunt, J.W. Yan, Q.Q. Han, H.X. Zhu, S. Bigot, W.F. He, Softening and hardening on a Zr-based bulk metallic glass induced by nanosecond laser surface melting, Mater. Sci. Eng. A 803 (2020), 140497.
[45] H. Huang, J. Noguchi, J.W. Yan, Shield gas induced cracks during nanosecond-pulsed laser irradiation of Zr-based metallic glass, Appl. Phys. A Mater. Sci. Process. 122 (2016) 881.
[46] H. Huang, J.W. Yan, Investigating shear band interaction in metallic glasses by adjacent nanoindentation, Mater. Sci. Eng. A 704 (2017) 375–385.
[47] C. Schuh, T. Hufnagel, U. Ramamurty, Mechanical behavior of amorphous alloys, Acta Mater. 55 (2007) 4067–4109.